COMPOUND SEMICONDUCTOR APPLICATIONS FOR AUTOMOTIVE SENSORS

M. W. Pelczynski, J. J. Heremans* and S. Schwed, EMCORE Corporation, Somerset, NJ
*Present address: Department of Physics and Astronomy, Ohio University, Athens, OH 45701

ABSTRACT

Compound semiconductors find extensive application as magnetic position sensors in the automotive environment. Typical applications involve the sensor element, a permanent magnet attached to the sensor, and a moving magnetic circuit –a target wheel. Wider mechanical gaps in the magnetic circuit can be utilized with a sensor of higher sensitivity, and thus high sensitivity is valuable. Further limitations on the choice of materials are imposed by temperature sensitivity, as the automotive environment is characterized by wide temperature operating ranges (-40°C up to 200°C). The magnetic signal may be hidden by the temperature drift in the sensor output, and thus temperature stability limits the sensor's resolution. Automotive position sensors find use in ignition timing and misfire detection (cam and crank sensors), as wheel speed sensors (anti-lock brakes and other types of active wheel-control), in brushless electric motors and several other applications. This work reviews progress achieved to refine the use of InSb for automotive sensing applications.

INTRODUCTION

Magnetic sensors for automotive applications often require the ruggedness inherent in semiconductor devices. Moreover, semiconductor devices typically operate at voltage and current levels compatible with electronic components already present (microprocessors, oxygen sensors etc.). Semiconductor magnetic sensors derive their sensitivity mainly from two parameters: the device geometry, and the material's mobility.

Two geometries have found application [1, 2]: the Hall geometry and the magnetoresistor (or Corbino) geometry (Fig. 1). In the Hall geometry, Fig. 1(a), a driving signal (voltage or current) is applied to two input contacts, and the output signal consists of the Hall voltage resulting from the transverse component of the resistivity tensor. The Hall voltage, V_H, appears at two voltage contacts, separate from the driving contacts and is given by $V_H = IB / (net)$, where I is the current through the device, B is the applied magnetic field, n is the carrier concentration, t is the thickness of the semiconductor layer and e is the electron charge. Using the expression for the device resistance, we can write V_H in terms of the driving voltage, V_{in} , as $V_H = V_{in}\ \mu\ (W/L)$ whereby μ is the material mobility, W is the width of the Hall device and L its effective electric length. Since for InSb, as we will discuss, the density n displays a sharper temperature dependence than the mobility μ, a constant voltage rather than a constant current is often used to drive the Hall sensor. In the former case, the output signal V_H is proportional to μ. In the constant current drive case, although μ does not appear directly in the expression for V_H, mobility is still the dominant factor determining the signal-to-noise ratio [3].

The second geometry, magnetoresistor, is depicted in Fig.1(b). Unlike Hall devices, magnetoresistors are nearly always utilized as two-terminal devices. The current path is very short compared to Hall devices, and the very short path, together with the wide current contacts, hinders the development of a transverse Hall voltage. Instead, the device resistance displays a quadratic dependence on magnetic field: $R = R_0\ (1+g(\mu B)^2)$, where R_0 is the zero-field resistance at a given temperature, and g is a geometrical factor ($g \sim 0.8$). Thus, the magnetic field dependence is once more determined by the mobility μ of the material. Obviously, in either geometry, μ determines the usefulness of a given material for magnetic sensing applications. Moreover, in the case of epitaxial material, this mobility should be achieved with as thin an

Mat. Res. Soc. Symp. Proc. Vol. 607 © 2000 Materials Research Society

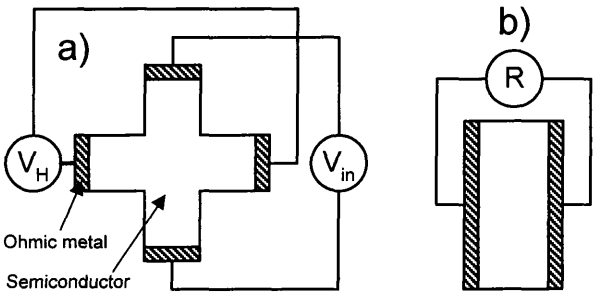

Figure 1: Semiconductor magnetic sensor geometries: a) Hall geometry (4-contact), illustrated under constant driving voltage (V_{in}) conditions, and b) magnetoresistor geometry (2-contact), illustrated as a resistance measurement (practical magnetoresistors are composed of a series combination of such elements).

active region as possible to increase the device resistance and thus minimize current and power consumption. Most of the work described here has focused on achieving these contradictory dictates on InSb.

Materials often encountered in magnetic sensor applications are Si, GaAs, InAs and InSb, in order of increasing μ. Si, always used in the Hall geometry, enjoys the advantage of very mature processing technology but, when used as a magnetic sensor, suffers considerable disadvantages because of its low mobility, and its sensitivity to piezo-electrically induced offsets [1, 4]. Cancellation of these effects necessitates the use of complex multiple-plate Hall geometries, whereas the low μ translates to low sensitivity, requiring substantial on-chip amplification and other signal processing [4]. Thus, Si Hall plates are almost always integrated with other circuit components, required to mitigate its drawbacks, into a monolithic sensor. Despite the complexity, many hurdles have been overcome, and integrated Si Hall sensors form a large part of the market. GaAs, InGaAs and InAs [5, 6], almost always used in the Hall geometry, have not yet appeared in integrated devices. Both materials enjoy substantially higher mobilities than Si [7], and this allows the fabrication of very small, low cost, simple, low-noise and sensitive sensors, often used as position sensors in brushless motors found in consumer electronics (disk drives, camcorders,...). InSb enjoys the highest mobility of III-V semiconductors (at room temperature μ ranges up to 78,000 cm^2/Vs in bulk material, 60,000 cm^2/Vs in epitaxial form), and therefore forms the ideal choice for magnetic sensors. However, in InSb and other narrow bandgap semiconductors, the intrinsic carrier density is strongly dependent on temperature. Unless controlled by judicious doping, epitaxial layer sequence and circuit topology, the temperature sensitivity causes a strong temperature variation of the device response and would limit narrow bandgap sensors to operation close to room temperature, precluding their use in the automotive environment. We will discuss the developments that have designated InSb as the epitaxial material of choice for automotive magnetic position sensors.

EXPERIMENT

Epitaxial InSb has been grown by metal-organic chemical vapor deposition (MOCVD) on GaAs or Si substrates in two EMCORE reactors. To test the possibility of an integrated III-V

magnetic sensor device, InSb was also deposited on heterojunction bipolar transistor (HBT) material, consisting of a GaAs substrate and a combination of GaAs and InGaP layers lattice matched to GaAs. Throughout this work either 4" semi-insulating GaAs substrates cut 2° off-axis, or 4" Si substrates cut 4° - 6° off-axis have been used. The Si substrates were ordered with a specially large resistivity (5 - 60 kΩ-cm) to prevent shunting of the InSb devices through the substrate throughout the temperature range of interest. Growths for this work were performed on EMCORE D180 and E400 MOCVD systems. The D180 and E400 systems are vertical chamber, low-pressure MOCVD reactors, characterized by high susceptor rotational speeds (Turbo-disc technology) and resistively heated susceptors. In several cases, modified inlet flow flanges have been employed to obtain optimized gas reaction conditions. The epitaxial material of different designs was characterized by magnetotransport measurements in a variable temperature cryostat. Samples from the material were fabricated into van der Pauw geometries [8] and magnetotransport measurements yielded carrier density and mobility as a function of temperature from 77 K to 460 K (the magnetic fields used ranged from – 0.8 T to 0.8 T). After optimization of the epitaxial design, magnetoresistor and Hall devices were fabricated. The device fabrication process involves photolithography and wet etching for mesa definition, metal stack evaporation for Ohmic contact formation, and Si_3N_4/SiO_2 passivation. Finished devices were characterized as magnetic sensors over temperature (77 K to 460 K) and magnetic field (typically –0.5 T to 0.5 T). For both Hall devices and magnetoresistors, we thus obtained device sensitivity and device resistance. Magnetoresistors find application as dual elements, whereby two matched devices are employed in a bridge configuration. Such dual element configuration reduces the temperature sensitivity, but creates stringent device matching conditions [9]. For manufacturing simplicity, device pairs are defined as neighboring devices and thus, device matching is obtained through wafer homogeneity. Magnetoresistors are thus characterized as a pair, and mismatch is measured as well. For Hall devices, often used as single elements, the corresponding measurement is offset voltage (the Hall voltage output at zero magnetic field) [4]. Of particular importance are mismatch drift and offset drift with temperature, as both mismatch and offset alone can be electronically nulled. Temperature drifts, however, fundamentally limit the smallest magnetic field resolvable over a given temperature range, and thus limit the sensor resolution.

We will separately discuss several epitaxial InSb designs, optimized for different applications.

InSb on GaAs

The InSb wafers described in this section are intended for large scale commercial production of magnetoresistors and Hall devices. "Epi-ready" GaAs substrates are loaded into the reactor through a load lock, and prior to growth, heated to 700°C for 10 mins., and cooled to growth temperature under arsine flow. For InSb growths, trimethylindium (TMIn) and

Table I: Growth Parameters

Material	Sources	Source Temperature (C)	Source Pressure (Torr)	Growth Pressure (Torr)	Growth Temperature (C)	V/III Ratio	Growth Rate (μm/hr)
n- GaAs	TMGa, AsH3	-14	425	35	600	70	3
InSb	TMIn, TRIS	20, 25	429, 323	35	395	6.5	0.9
p+ GaAs	TMGa, AsH3	-14	425	35	600	30	3
InAlSb	TMIn, TESb, TTBAL	20, 25, 30	429, 450, 400	150	450	1.5	0.6
GaAs (nuc)	TEGa, AsH3	25	1000	35	325	500	0.4

trisdimethylaminoantimony (TRIS) [10] were used as In and Sb precursors respectively, and diethyltellurium in H_2 is used as the Te n-type dopant source [11]. Table I contains typical InSb growth conditions for the structures discussed in this work. For each epitaxial design, we optimized growth conditions by varying the growth temperature and the V-III ratio, guided by figures of merit such as surface specularity, X-ray diffraction full-width-at-half-maximum (XFWHM) and, above all, mobility and device characteristics. The optimum growth temperature for InSb was found to be ~ 395°C.

Figure 2 shows the Hall output voltage, under constant driving voltage (V_{in}) conditions, plotted as V_H/V_{in}, for Hall sensors fabricated from different epitaxial materials. The data was obtained at B = 0.05 T and V_{in} = 1.0 V. Since $V_H = V_{in}\ \mu$ (W/L), which for the particular conditions in the figure reduces to $V_H/V_{in} = 0.4\ \mu B$, we see that the ordinate in Fig. 2 directly reflects μ (plotted *vs.* temperature T). The trace labeled D131 refers to epitaxial InSb, 0.80 μm thick, grown on GaAs substrate, and n-type Te doped to $2.4x10^{16}$ cm^{-3}. For InSb, this doping yields material slightly n-type at room temperature, as the intrinsic carrier concentration ~ $1.8x10^{16}$ cm^{-3} at that temperature. The slight n-doping was deliberately achieved to mitigate the dependence of transport parameters on T observed for narrow bandgap intrinsic material, and to avoid magnetotransport type inversion intrinsic material may experience when cooled. Type inversion brings a precipitous decline in μ, as the heavy-hole mobility is a factor 90 times smaller than the electron mobility in InSb. The trace labeled D134 refers to material grown under identical conditions to D131, but of reduced thickness: 0.70 μm for D134 compared to

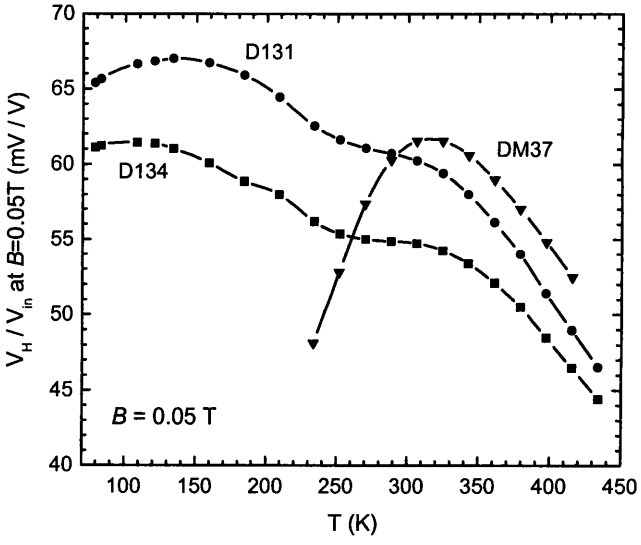

Figure 2: $V_H/V_{in} \sim \mu$ vs. T at B = 0.05 T for Hall devices fabricated on GaAs substrate: 1) D131: 0.15 μm undoped InSb buffer, 0.80 μm InSb n-type Te doped to $2.4x10^{16}$ cm^{-3}; 2) D134: 0.15 μm undoped InSb buffer, 0.70 μm InSb n-type Te doped to $2.4x10^{16}$ cm^{-3}; 3) DM37: 0.80 μm InSb, nominally undoped.

0.80 μm for D131. The observed reduction in μ as a function of thickness is expected, as the average μ of thinner material is more heavily influenced by the disordered GaAs/InSb interface. Lattice mismatch (14%) at this interface leads to formation of threading dislocations, which both reduce the mobility of the interface layer and function as n-type dopants [12]. One thus expects a depressed average μ as accessed by the magnetotransport measurements. The disordered interface layer presents an additional reason to provide n-type doping in the active layer: the dislocation-doped low-μ interface layer may otherwise shunt the high-μ active layer, leading to low effective layer mobilities. In fact, to reduce the shunting effect due to the interface layer, our epitaxial designs routinely incorporate a deliberate reduction of Te doping at the initial stages of growth, thus providing a nominally undoped buffer layer. Both D131 and D134 incorporate such undoped buffer, of nominal thickness 0.15 μm.

The trace labeled DM37 in Fig. 2 illustrates a nominally undoped, 0.80 μm thick InSb layer (i.e. not including a buffer layer). Comparison between DM37 and D131 shows the effect of the slight Te doping present in D131. Different scattering mechanisms dominate at different temperatures: at low T (~ < 200 K), ionized impurity scattering dominates, and is induced by the interface dislocations as well as the intentional n-type dopants. At higher T (~ 200 K < T < 450 K), polar longitudinal optical phonon scattering determines the mobility, whereas at the highest T (~ > 450 K), electron - heavy-hole scattering dominates [13]. Consistent with these mechanisms, the undoped DM37 sample's μ drops sharply at lower T, but remains higher than the doped samples' μ at higher T where the comparative lack of ionized impurity scattering compensates. All three samples should be equivalently sensitive to phonon scattering mechanisms. The two-maximum structure observed in the mobility in traces D131 and D134 is attributed to the competing effects of different scattering mechanisms. The high T maximum around 320 K is preserved for undoped material. A detailed description of these features has not yet been achieved. Although, as Fig. 2 indicates, epitaxial material for Hall device applications should contain n-type doping, the doping levels should remain low. Indeed, high doping levels lead to low device resistance and for devices operating under constant driving voltage, this causes high current consumption. Thicker epitaxial layers, enticing to increase the average mobility, suffer the same drawback. Indeed device resistance is proportional, within a geometrical factor, to the material's sheet resistance, $R_S = 1/(ne\mu t)$. Thus, Hall device applications should strive for thin epitaxial layers displaying high mobility and low doping. As these requirements are contradictory, best results will be obtained as a compromise.

Figure 3 contains mobility and density *vs.* T for three different epitaxial designs on GaAs substrates. The trace labeled MR applies to material optimized for magnetoresistor applications . Magnetoresistor material allows less stringent limits on device resistance, providing opportunities for enhancing μ by increasing the layer thickness *t*. Doping can be increased as well, affording device resistances less dependent on T. The material corresponding to the MR trace consists of a 0.2 μm, $4x10^{16}$ cm^{-3} Te-doped InSb buffer layer, grown on GaAs substrate, followed by a 1.3 μm, $1x10^{17}$ cm^{-3} Te-doped InSb active layer, capped by a 0.05 μm, $3x10^{17}$ cm^{-3} Te-doped InSb contacting layer (designed to facilitate Ohmic contact formation). The mobility represents average values for the layer stack. As discussed above, the buffer layer mitigates the effect of the dislocated interface layer. The active layer's design optimizes μ and temperature stability.

Figure 4 (upper panel) contains magnetoresistor characteristics (resistance R *vs. B*), parametrized in T, for devices fabricated utilizing this material. As expected, R is a quadratic function of *B* (at low *B*). The curves flatten and lower for increasing temperatures, due to a decreasing μ and decreasing sheet resistance. Since magnetoresistors are designed for use in a

Wheatstone bridge configuration, where one arm of the bridge consists of a pair of matched magnetoresistors, of more relevance is the sensitivity S, defined as S = (1/R) (dR/dB), displayed as a function B, parametrized in T, in the lower panel of Fig. 4. Indeed the voltage imbalance of such bridge circuit, when a magnetic field B is applied to one member of the magnetoresistor pair and $B + \Delta B$ to the other member, is given by $\Delta V = S\ \Delta B\ V_b$, where V_b is the bridge driving voltage. Thus, S determines the output of the bridge circuit. The magnetoresistors should be biased by a permanent magnet (often SmCo) up to the value of B where S reaches its maximum for the temperatures of interest (~ 0.25 T). Finally, the inset to Fig. 4 shows the mismatch, computed in units of B (Gauss), for a magnetoresistor pair (the data in the main panels refers to one member of this pair). Indeed, an imbalance in resistance between the pair is interpreted by the external electronics as arising from a magnetic field difference, ΔB. The mismatch can be nulled at one specific T. Therefore, the variation over temperature and bias field of this mismatch forms an expression for the attainable resolution. The resolution is properly specified for a range of operating T and B: e. g. for the pair in Fig. 4, the resolution for -40°C < T < 175°C and for 0.2 T < B < 0.4 T is ~ 1.5 G.

Returning to Fig. 3, trace LA679 refers to a low doped version of the material represented by the trace MR. LA679 consists of a 0.2 μm, undoped InSb buffer layer, grown on GaAs substrate, followed by a 1.3 μm, $3x10^{16}$ cm^{-3} Te-doped InSb active layer, capped by a 0.05 μm, $1.5x10^{17}$ cm^{-3} Te-doped InSb contacting layer. Thus, compared to the material MR, the doping in the active layer of LA679 is reduced. This leads to a higher mobility, especially at lower T.

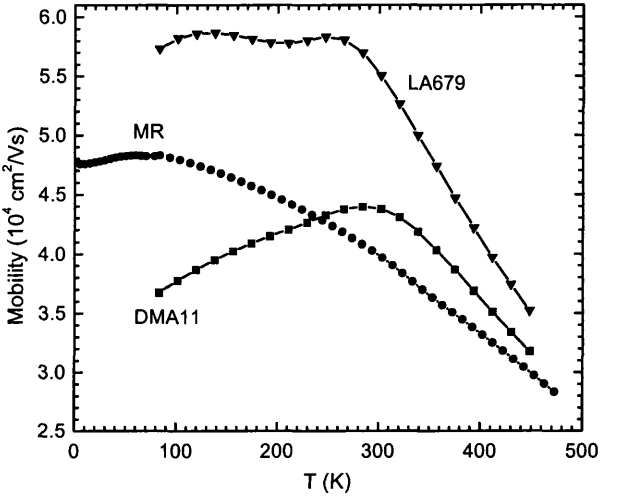

Figure 3: Mobility vs. T for InSb on GaAs substrate 1) MR: 0.2 μm $4x10^{16}$ cm^{-3} Te-doped InSb buffer, 1.3 μm $1x10^{17}$ cm^{-3} Te-doped InSb active, 0.05 μm $3x10^{17}$ cm^{-3} Te-doped InSb cap; 2) LA679: 0.2 μm undoped InSb buffer, 1.3 μm $3x10^{16}$ cm^{-3} Te-doped InSb active, 0.05 μm $1.5x10^{17}$ cm^{-3} Te-doped InSb cap and 3) DMA11: 0.15 μm undoped InSb buffer, 0.6 μm $3x10^{16}$ cm^{-3} Te-doped InSb active, 0.05 μm $1.5x10^{17}$ cm^{-3} Te-doped InSb cap.

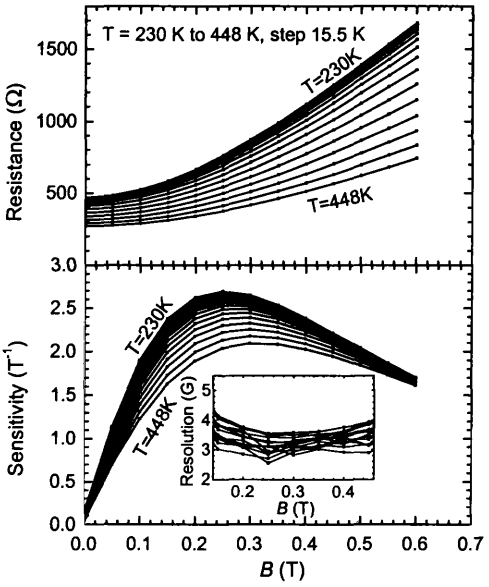

Figure 4: Magnetoresistor characteristics for devices fabricated on material MR (Fig. 3). Upper panel: resistance R vs. B, parametrized in T. Lower panel: sensitivity (1/R) dR/dB vs. B parametrized in T (devices are optimized for operation near the maximum at B ≈ 0.25 T). Inset: T-drift limited resolution of a magnetoresistor pair, over a range of B, parametrized in T.

The T-dependence of both μ and density at higher T has deteriorated, however. The mobility displays the double maximum also observed for samples of similar doping in Fig. 2. For comparison, Fig. 3 also includes data for a thin and low doped design, DMA11, consisting of a 0.15 μm, undoped InSb buffer layer, grown on GaAs substrate, followed by a 0.6 μm, $3x10^{16}$ cm^{-3} Te-doped InSb active layer, capped by a 0.05 μm, $1.5x10^{17}$ cm^{-3} Te-doped InSb contacting layer. This structure shares doping levels with LA679, but its active layer has been approximately halved. The effect on μ of the reduced thickness is evident from the data. Intriguingly, this structure's mobility displays a single maximum, similar to DM37 in Fig. 2.

InSb/InAlSb on GaAs

The disordered interface layer between GaAs and InSb has led us to a search for a buffer layer capable of reducing the dislocation density in the InSb layers, and sufficiently resistive not to contribute to the average mobility of the layer stack. $In_{1-x}Al_xSb$, although not lattice matched to InSb, represents a suitable candidate [14]. At low Al mole fraction x, $In_{1-x}Al_xSb$ offers a lower mismatch to InSb whereas at higher x the material displays a larger bandgap and thus higher resistivity.

We have demonstrated the first large area growth of $In_{1-x}Al_xSb$ by MOCVD, obtaining specular growth over the entire surface of a 4" GaAs wafer. Precursors used were TMIn, tritertiarybutylaluminum (TTBAL), and triethylantimony (TESb). Table I contains the growth parameters. In order to overcome the significant MOCVD prereactions occuring in this material

system, it is necessary to use large flows of both TTBAL and TESb to achieve reasonable growth rates. We also found it necessary to apply high push flows and low alkyl manifold line pressure to increase the gas velocity and decrease available prereaction time. Finally, higher growth pressures (> 100 Torr) were necessary to achieve acceptable morphologies. It was realized that modifying x required adjustment of the Sb molar flow as well, to achieve specular growth, due to the prereactions. As a matter of choice we utilized x = 0.28 for the $In_{1-x}Al_xSb$ buffer layers. The mole fraction x was verified by X-ray diffraction (by resolving the 311 and 400 spectra), as well as SIMS measurements.

Figure 5 illustrates the effect on mobility of a variety of buffer layers, including the $In_{1-x}Al_xSb$ layers described above. The samples described all contain a thin active layer (0.4 μm, compared to 1.0 μm for wafer MR of Figs. 3-4). As mentioned, thin active layers require efficient buffer layers to maintain mobility. Sample LA585 does not contain a buffer layer, and consists of a 0.4 μm, $1x10^{17}$ cm^{-3} Te-doped InSb active layer, capped by a 0.05 μm, $3x10^{17}$ cm^{-3} Te-doped InSb contacting layer. Sample LA586 contains a 0.25 μm nominally undoped InSb buffer layer, followed by a 0.4 μm, $1x10^{17}$ cm^{-3} Te-doped InSb active layer, capped by a 0.05 μm, $3x10^{17}$ cm^{-3} Te-doped InSb contacting layer. Sample LA425, finally contains a 0.2 μm nominally undoped $In_{0.72}Al_{0.28}Sb$ buffer layer, followed by a 0.4 μm, $1x10^{17}$ cm^{-3} Te-doped InSb active layer, capped by a 0.05 μm, $3x10^{17}$ cm^{-3} Te-doped InSb contacting layer. LA585, lacking a buffer layer, exhibits the lowest μ, throughout the range of T. Its density (inset to Fig. 5) is also the highest, pointing to the existence of dislocations throughout the structure. The mobility

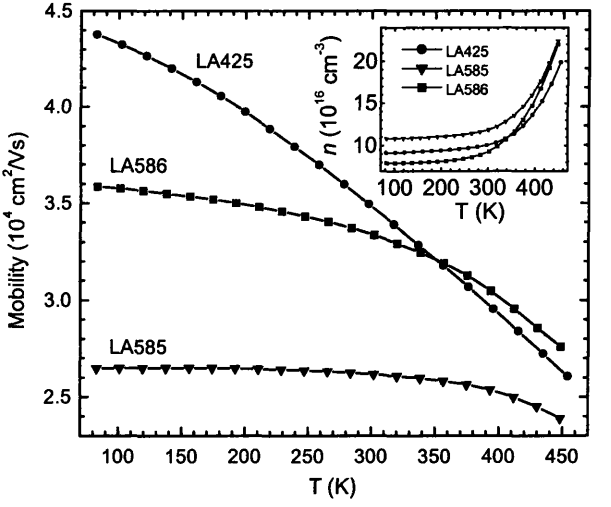

Figure 5: Mobility vs. T for thin active InSb layers (InSb/InAlSb buffer study): 1) LA585: no buffer, 0.4 μm $1x10^{17}$ cm^{-3} Te-doped InSb active, 0.05 μm $3x10^{17}$ cm^{-3} Te-doped InSb cap; 2) LA586: 0.25 μm nominally undoped InSb buffer, 0.4 μm $1x10^{17}$ cm^{-3} Te-doped InSb active, 0.05 μm $3x10^{17}$ cm^{-3} Te-doped InSb cap; 3) LA425: 0.2 μm nominally undoped $In_{0.72}Al_{0.28}Sb$ buffer, 0.4 μm $1x10^{17}$ cm^{-3} Te-doped InSb active, 0.05 μm $3x10^{17}$ cm^{-3} Te-doped InSb cap. Inset: carrier density, n.

maintains a flat profile over this range, since scattering is dominated by dislocations. LA586 shows a substantially improved μ, with similar, but more pronounced temperature dependence. The sample containing the $In_{0.72}Al_{0.28}Sb$ buffer layer, LA425 exhibits improved μ at lower T. Its T dependence deviates qualitatively at lower temperatures,, pointing to the dominance of different scattering mechanisms in this range. We attribute these observations to the effectiveness of the $In_{0.72}Al_{0.28}Sb$ buffer layer in preventing dislocation-dominated scattering. As previously pointed out, at low T we expect dislocation induced scattering and ionized impurity scattering to dominate, whereas at higher T phonon scattering dominates. Thus, the relative absence of dislocations should appear particularly clearly at lower T, as evidenced in Fig. 5. Moreover, at higher T, all samples should qualitatively revert to the same T dependence, as observed. We conclude that the $In_{0.72}Al_{0.28}Sb$ buffer indeed effectively protects the transport properties from the effects of interface disorder. Although magnetoresistor devices fabricated from LA425 material exhibited excellent properties, the difficulty of $In_{1-x}Al_xSb$ growth has prevented us from fully exploiting this benefit. Further studies varying the doping level in the active layers have shown that, in this case also, Te doping of $1x10^{17}$ cm^{-3} yields an ideal balance between high μ, acceptable sheet resistance and temperature stability for magnetoresistor pair applications.

InSb on Si

GaAs substrates offer the advantage of high resistivity, protecting the devices from the parasitic effects engendered by current shunting. However, compared to Si, GaAs substrates suffer from high cost, fragility and large wafer thickness (thin GaAs is deemed too fragile for production environments). Thus, small die suffer from extreme dimensional aspect ratios and processed wafers often need to be thinned to fit into standard low profile packages. This thinning step, in turn, reduces yields and increases cost. Thus, effort have been spent to develop hetero-epitaxial growth of a variety of III-V compounds on Si substrates. We will discuss the characteristics of InSb growth on Si substrates.

InSb hetero-epitaxy on Si presents several challenges. The InSb - Si lattice mismatch is 19 % (compared to 14 % for GaAs), placing extreme demands on the buffer layers. The buffer layers also must prevent current shunting through the substrate, since Si, even in high resistivity form, displays a resistivity lower than GaAs' due to its smaller bandgap. Finally, the polar III-V compounds form anti-phase domains (APDs) when deposited on non-polar Si. As we will discuss, anti-phase domains apparently do not drastically influence the magnetotransport properties in InSb, in contrast to their well-known deleterious effects on opto-electronic devices. Thus, magnetic sensors, based on magnetotransport properties, may form a suitable objective for hetero-epitaxial growth on Si.

High resistivity Si ($\rho > 14$ kΩ-cm) substrates were prepared prior to growth by etching in buffered oxide etch for 1 min. and were introduced in the MOCVD reactor through a loadlock. The substrates were then heated to about 800°C for 20 mins. under excess arsine and cooled to growth temperature. A GaAs layer was nucleated as a template for subsequent GaAs buffer layer growth, exploiting previous knowledge of InSb growth on GaAs. This GaAs buffer layer must display sufficient sheet resistance (to prevent shunting) and satisfactory morphological characteristics (as it used as a starting point for the InSb epitaxy). A study was performed in order to optimize the GaAs buffer layer growth, utilizing as figures of merit XFWHM, sheet resistance and surface haze. The buffers employed possessed a tri-layer structure: a low temperature GaAs nucleation layer, followed by a layer during which the temperature was ramped up, and a final GaAs cap layer. Parameters varied to optimize the figures of merit included the nucleation temperature, the nucleation layer thickness, the temperature ramp

method (growth / no growth during ramp), the temperature ramp layer thickness (in the case of growth, above), the V/III ratio and the Si substrate misorientation. In short, from the buffer study we concluded that lower nucleation temperatures lead to lower X-ray XFWHM and that 5° Si misorientation formed the best compromise between morphology and APD formation.
Moreover, XFWHM decreases as the temperature ramp growth time is increased, whereas sheet resistance increases with lengthening nucleation layer growth time. These observations allowed us to produce optimized GaAs buffers, as platforms for rather standard InSb layer growth. The optimized InSb growth parameters are shown in Table I. Figure 6 contains a comparison between μ and carrier density *vs.* T, obtained for InSb on GaAs and InSb on Si substrates. The InSb structures were nominally identical and of the same structure as MR in Fig. 3. The material carrier densities are comparable (the wafers were grown in different reactors, and the difference in density can be accounted for from the difference in dopant flow calibration). The T behavior of μ, however, merits consideration. At higher T, both mobilities follow very similar dependencies and moreover display quite similar values. At lower T, a deviation occurs, reducing μ of the Si-substrate sample. This is consistent with our expectations: the larger mismatch, perhaps aided by APD formation, reduces μ at lower T, where dislocation scattering dominates. The reduction in μ is not drastic, reflecting the effectiveness of the GaAs buffer layer. Although the Si-substrate sample suffers from enhanced dislocation scattering, the mobility at high T is still dominated by phonon processes. Since, in automotive applications, particular attention is paid to retention of device characteristics at higher T, we conclude that InSb on Si substrates indeed forms suitable magnetic sensor material. We also performed thermal shock testing (rapid and repeated temperature cycling from 77 K to 473 K), and observed that such severe test does not lead to film peel and indeed only reduces μ by about 3 %. Further, no increased mismatch drift was observed in fully processed magnetoresistors, while sensitivities suffered only slight reduction compared to equivalent GaAs-substrate devices. Part

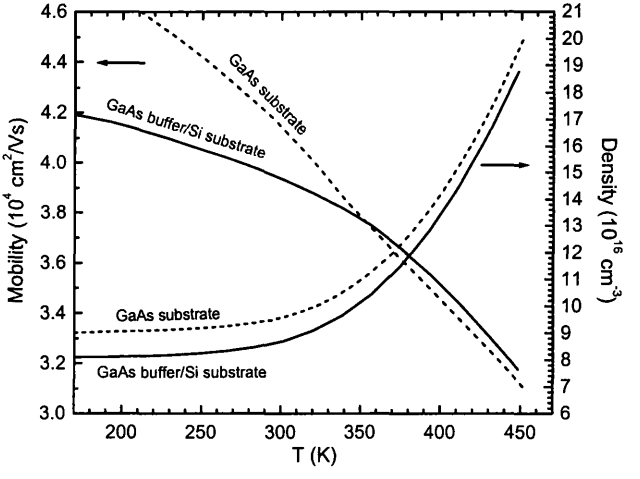

Figure 6: Mobility and carrier density comparison between InSb on Si substrate / GaAs buffer and InSb on GaAs substrate. Both InSb structures were nominally composed of a 0.2 μm $4x10^{16}$ cm^{-3} Te-doped InSb buffer, 1.3 μm $1x10^{17}$ cm^{-3} Te-doped InSb active and 0.05 μm $3x10^{17}$ cm^{-3} Te-doped InSb cap.

of the small loss in S is due to current shunting through the Si substrate. To quantify this effect, we utilized the room temperature ratio of the resistance from adjacent devices to the internal device resistance, normalized to sheet resistance. For high-ρ Si (>14 kΩ-cm), this ratio ≈ 200, corresponding to a current loss of about 0.5 % and translating to a loss in S of the same, negligible, magnitude. Magnetoresistor characterization (similar to Fig. 4) over T up to 180°C yielded similarly satisfactory device characteristics.

InSb on heterojunction bipolar transistor material

Peripheral electronic circuitry must provide power and signal conditioning to the sensing element. In many cases, the circuitry is provided by a Si ASIC, packaged together with the magnetoresistor pair or Hall element and a biasing magnet. Si Hall plates are often integrated with the associated electronics into a single IC. With the advent of mature III-V HBT technology, the same approach has become accessible for InSb sensors, whereby the InSb sensing layer is grown on top of the HBT material and InSb and HBT circuitry are subsequently processed into monolithically integrated sensors. Advantages of this approach include the large signal-to-noise gain achievable with high-μ III-V sensors compared to Si and extended temperature capability. A development program toward such sensors has been initiated at EMCORE, utilizing InGaP HBT technology [see e.g. Ref. 15] and focusing on the development of a suitable buffer between the HBT and InSb. The buffer requirements are similar to those previously encountered: lattice matched to the HBT (i. e. lattice matched to GaAs), and of sufficient resistivity to prevent shunting of the sensor through the HBT.

We have experimented with three separate buffer structures: 1) 2 μm of n-GaAs (< 5 x 10^{14} cm^{-3}); 2) a 20 period $Al_xGa_{1-x}As/GaAs$ superlattice with x ≈ 0.24, followed by a 1.7 μm n-GaAs layer; and 3) 1 μm of n-GaAs and 0.2 μm of p^+ doped GaAs (4 x 10^{19} cm^{-3}), followed by a 1 μm n-GaAs layer. Table I contains the growth parameters. Besides buffer morphology, current shunting through the HBT structure was used as a figure of merit, utilizing the approach outlined for the Si substrate devices. Shunting ratios for the different buffer structures were measured at 1100 for buffer #1, at 7.0 for buffer #2 and at 1.0 for buffer #3, clearly eliminating the last two structures. Thus, the n-GaAs buffer leads to a negligible loss in S due to shunting, of about 0.1%. High T magnetoresistor characterization showed S values ~ 10% lower than those obtained for InSb on GaAs devices, due to slight mobility deterioration. This small loss in S is inconsequential in the light of the amplification and signal processing provided by the underlying HBT circuitry.

CONCLUSIONS

InSb magnetoresistors and Hall devices exhibit excellent sensor characteristics due to the high mobility of the material. Ideal magnetic sensor material displays high mobility, high sheet resistance and sufficiently small temperature coefficients, a combination that requires careful epitaxial design and poses stringent requirements on buffer layers between substrates and InSb. Moreover, these transport parameters, in addition to tight device matching characteristics, must be maintained over a wide temperature range (-40°C to 200°C), despite the narrow bandgap nature of InSb. We described the MOCVD growth of InSb on various substrates, with emphasis on maintaining mobility, carrier density and sheet resistance to within prescribed limits over this wide temperature range. Utilizing optimized InSb, InAlSb or GaAs buffers, we describe high-mobility InSb obtained on GaAs substrates, high resistivity Si substrates and heterojunction bipolar transistor epitaxial material. The InSb layer structure is either optimized for magnetoresistor or Hall device applications. InSb hetero-epitaxy on Si substrates offers

economic or packaging flexibility, whereas growth on heterojunction bipolar transistor epitaxial material opens wide avenues towards monolithically integrated III-V magnetic sensors.

ACKNOWLEDGMENTS

The authors acknowledge enlightening discussions with J. P. Heremans. Production of exploratory devices was made possible through the cooperation of E. Douglas, C. W. Farley and P. Cooke.

REFERENCES

1) R. S. Popović, *Hall Effect Devices* (Adam Hilger, Bristol, 1991); Sens. Act. A **56**, 39 (1996).

2) H. H. Wieder, *Hall Generators and Magnetoresistors* (Pion Ltd. London, 1971) pp. 17 – 47.

3) H. M. J. Vaes and T. G. M. Kleinpenning, J. Appl. Phys. **48**, 5131 (1977).

4) R. S. Popović and B. Hälg, Solid State Electronics **31**, 1681 (1988); H. Blanchard, C. de Raad Iseli and R. S. Popović, Sens. Act. A **60**, 10 (1997).

5) M. Behet, J. Das, J. De Boeck and G. Borghs, IEEE Trans. Magn. **34**, 1300 (1998).

6) J. S. Lee, K.-H. Ahn, Y.-H. Jeong and D. M. Kim, Sens. Act A **57**, 183 (1996).

7) J. Heremans, J. Phys. D: Appl. Phys. **26**, 1149 (1993).

8) L. J. van der Pauw, Philips Res. Repts. **13**, 1 (1958).

9) J. P. Heremans, Mater. Res. Soc. Proc. **475**, 63 (1997).

10) J. Shin, Y. Hsu, T. C. Hsu and G. B. Stringfellow, J. Elec. Mat. **24**, 1563 (1995).

11) D. L. Partin, M. Pelczynski, P. Cooke, L. Green, J. Heremans and C. M. Thrush, J. Cryst. Growth **195,** 378 (1998).

12) D. L. Partin, J. Heremans and C. M. Thrush, Sens. Act. A **69**, 39 (1998).

13) W. Zawadzki and W. Szymanska, J. Phys. Chem. Solids **32**, 1151 (1971).

14) D. L. Partin, J. Heremans and C. M. Thrush, J. Vac. Sci. Technol B **17**, 1267 (1998).

15) Compound Semiconductor **4**, pp. 4-5 (1998).